

Quantitative investigation of the multiphoton intrapulse interference phase scan method for simultaneous phase measurement and compensation of femtosecond laser pulses

Bingwei Xu, Jess M. Gunn, Johanna M. Dela Cruz, Vadim V. Lozovoy, and Marcos Dantus

*Department of Chemistry and Department of Physics and Astronomy, Michigan State University,
East Lansing, Michigan 48824*

Received May 6, 2005; revised August 12, 2005; accepted August 17, 2005; posted October 21, 2005 (Doc. ID 61987)

Femtosecond pulse characterization and compensation using multiphoton intrapulse interference phase scan (MIIPS) [Opt. Lett. **29**, 775 (2004)] was rigorously tested. MIIPS was found to have 3 mrad precision within the 90 nm bandwidth of the pulses. Group-velocity dispersion measurements of glass and quartz provided independent accuracy tests. Phase distortions from high-numerical-aperture objectives were measured and corrected using MIIPS, an important requirement for reproducible two-photon microscopy. Phase compensation greatly improved the pulse-shaping results through a more accurate delivery of continuous and binary phase functions to the sample. MIIPS measurements were possible through the scattering of biological tissue, a consideration for biomedical imaging. © 2006 Optical Society of America

OCIS codes: 320.0320, 320.7100.

1. INTRODUCTION

One of the critical aspects of using ultrashort-pulse lasers is controlling spectral phase distortions introduced by the interaction of the pulses with an optical surface such as a dielectric mirror or their transmission through dispersive media, such as a lens, an optical fiber, or a microscope objective. These distortions have a significant effect on the nonlinear properties of the pulse, leading to increased pulse duration, loss of peak intensity, and in some cases loss of information. The shorter the initial pulses, the more significant the distortions become, making the characterization and compensation of phase distortions in ultrashort pulses at the location where the laser meets the sample extremely important. Here we report on the quantitative performance of multiphoton intrapulse interference phase scan (MIIPS),^{1,2} a method that combines iterative spectral phase characterization and compensation, which we conclude is ideal for all nonlinear optical applications of femtosecond lasers.

Current established phase measurement methods include frequency-resolved optical gating (FROG)^{3–5} and spectral phase interferometry for direct electric field reconstruction (SPIDER).^{6–8} Unlike MIIPS, these methods, and their variants, depend upon the measurement of autocorrelations or cross correlations between two pulses to characterize the spectral phase of a pulse. In FROG, the frequency and time-resolved signals are used to retrieve the spectral phase of the pulses. SPIDER requires that the laser pulse be split into two beams that are then upconverted by a heavily chirped pulse. The interference of the upconverted pulses in the spectral domain is used to reconstruct the spectral phase in the original pulse.

Since the advent of ultrafast laser systems, the exciting field of ultrafast pulse shaping⁹ has spanned numerous

applications in optical communications,¹⁰ control of chemical reactions,^{11,12} nonlinear optical processes,^{13,14} semiconductors,¹⁵ quantum¹⁶ and nonlinear optical¹⁷ computation, and biomedical applications.¹⁸ Ideally, characterization and pulse shaping can work together to produce pulses with a precisely determined phase function, such as a zero-phase or transform-limited (TL) pulse. The first attempts to achieve TL pulses based on feedback dependence on spectral phase used a genetic algorithm-controlled shaper for adaptive compression.^{19–27} Others implemented time-domain interferometry with an acousto-optic programmable filter.²⁸ These indirect methods are limited by the lack of sensitivity of the total nonlinear optical signal to phase deformations outside the full width at half-maximum (FWHM) of the spectrum. MIIPS takes advantage of the influence that phase modulation has on the probability of nonlinear optical processes at specific frequencies.^{29–32} It is a single-beam method that not only characterizes the spectral phase but also compensates for unwanted phase distortions and can deliver accurate user-specified phase functions at the location of a sample. It does not require beam splitters, interferometry, autocorrelation, or global optimization. From the MIIPS method, one can analytically obtain the spectral phase across the pulse. Consequently, this method has proven to be extremely powerful for the accurate and reproducible demonstration of selective microenvironment probing,² multiphoton microscopy,³³ functional imaging,^{34,35} and chemical agent identification^{36,37} using ultrashort phase-shaped pulses.

2. THEORY

In MIIPS, a well-known reference function, $f(\omega)$, is introduced by the pulse shaper to cancel, at least locally, dis-

tortions by the unknown spectral phase $\phi(\omega)$ of the pulse. The sum of the unknown phase and the reference phase is given by $\varphi(\omega) = \phi(\omega) + f(\omega)$. The second-harmonic-generation (SHG) spectrum resulting from the total phase $\varphi(\omega)$ can be used to retrieve $\phi(\omega)$ accurately, as described below. Assuming the use of a thin nonlinear crystal with a pulse that is a few optical cycles long,^{38,39} the spectral response and the susceptibility can be replaced by constants, and the SHG intensity $S^{(2)}$ at frequency 2ω can be written as an integral over the spectral amplitude $|E(\omega)|$ and phase $\varphi(\omega)$ of the pulse:

$$S^{(2)}(2\omega) \propto \left| \int |E(\omega + \Omega)| |E(\omega - \Omega)| \exp[i(\varphi(\omega + \Omega) + \varphi(\omega - \Omega))] d\Omega \right|^2. \quad (1)$$

According to relation (1), the signal is proportional to the integral of the product of a real positive kernel, $|E(\omega + \Omega)| |E(\omega - \Omega)|$, with the complex exponent of phase $\varphi(\omega + \Omega) + \varphi(\omega - \Omega)$. TL pulses ($\varphi=0$) generate the maximum intensity for a SHG spectrum because the oscillatory component of the integral is zero.

The phase modulation produced by all physical processes is typically a continuous function, allowing us to write a Taylor expansion around ω . The Taylor expansion of the sum of the phases at positive and negative detuning is

$$\varphi(\omega + \Omega) + \varphi(\omega - \Omega) = 2\varphi(\omega) + \varphi''(\omega)\Omega^2 + \dots + \frac{2}{(2n)!} \varphi^{2n'}(\omega)\Omega^{2n}, \quad (2)$$

where $\varphi^{n'}(\omega) \equiv d^n \varphi(\omega) / d\omega^n$. According to Eq. (2), the SHG spectrum is maximized when $\varphi(\omega + \Omega) + \varphi(\omega - \Omega)$ is zero. To first approximation, neglecting higher-order even terms, the SHG spectrum has a local maximum at ω when the second-order phase distortion $\varphi''(\omega)$ equals zero, i.e., when $\varphi''(\omega) = \varphi''(\omega) + f''(\omega) \rightarrow 0$. At this frequency, $f''(\omega)$ compensates $\varphi''(\omega)$, and the unknown function $\varphi''(\omega)$ can be retrieved.

To measure the phase distortion across the spectrum, the reference function $f(\omega)$ is parameterized as $f(\delta, \omega)$, where δ is a parameter that is scanned, so that the reference function samples all frequencies in the bandwidth. The resulting SHG spectrum, $SHG(\delta, 2\omega)$, reaches a maximum when $\varphi''[\delta_m(\omega), \omega] = \varphi''(\omega) + f''[\delta_m(\omega), \omega] \rightarrow 0$ or $\varphi''(\omega) = -f''[\delta_m(\omega), \omega]$, where $\delta_m(\omega)$ denotes the δ value of the SHG maximum for each frequency. The phase of the pulse across the whole spectrum $\phi(\omega)$ can be analytically retrieved by double integration of $\varphi''(\omega)$ in the frequency domain. SHG and MIIPS are not affected by the choice of integration constants, the relative phase ϕ^0 and linear term ϕ' .

3. EXPERIMENTAL IMPLEMENTATION

The experimental setup for MIIPS necessitates only a thin SHG crystal, a spectrometer, and a pulse shaper capable of accurately introducing spectral phase modulation (see Fig. 1). There are no beams to overlap in space and

time, and no moving parts. Most experiments were carried out with a titanium:sapphire oscillator (K&M Laboratories) capable of producing sub-10 fs pulses (110 nm FWHM) centered near 800 nm. The average power of the oscillator was 250 mW, with a repetition frequency of 97 MHz. An amplified titanium:sapphire laser (Spectra Physics Spitfire) producing 0.7 μ J, 40 fs pulses at a 1 kHz repetition rate was also used. A 10 μ m β -barium borate type I crystal was used for SHG, and the output was directed to a spectrometer with ~ 2 nm spectral resolution. The pulse shaper, consisting of two SF10 prisms, two 200 mm focal-length cylindrical mirrors, and a dual-mask spatial light modulator (SLM) (CRI, Inc., SLM-256), is based on the general design of Weiner.⁹ To achieve accurate phase delays, each pixel of the SLM was carefully calibrated by measuring the polarization-dependent transmission of light through each pixel. Pixel-by-pixel calibration is necessary because of the frequency dependence of the index of refraction values.

For the MIIPS measurements, a sine function was utilized as the reference, $f(\delta, \omega) = \alpha \sin(\gamma\omega - \delta)$, where α and γ are fixed parameters with values equal to 1.5π and the duration of the pulse, respectively. The phase shift δ is a parameter typically scanned from zero to 4π . MIIPS is not limited to the use of periodic functions; other functions can be used. However, the sine function is practical for SLM implementation due to the fact that the maximum amplitude is limited to 2α over all values of δ .

For most measurements, we used $\gamma = 1/\tau_{\text{pulse}} = 10$ fs, $\alpha = 1.5\pi$, and δ is scanned from 0 to 4π . The acquisition of a SHG spectrum for each step over this range results in two replicas of the MIIPS trace. From the acquired spectra, a two-dimensional plot for $SHG(\delta, \omega)$ is obtained (see the left panels of Fig. 2), where $\omega = \pi c / \lambda_{SHG}$. The value of $\delta_m(\omega)$ for each frequency is found, and from these values the second derivative of the unknown phase is calculated by

$$\varphi''(\omega) = \alpha \gamma^2 \sin[\gamma\omega - \delta_m^n(\omega)]. \quad (3)$$

There are multiple solutions (index n) of Eq. (3). Because of these multiple solutions, the range in which we search for the maxima of the SHG spectra must be specified.

The expected values of $\delta_m^n(\omega)$ for TL pulses can be found by substituting $\varphi''=0$ into Eq. (3), $\delta_m^n(\omega) = \gamma(\omega - \omega_0) + n\pi$, $n=0, \pm 1, \pm 2, \dots$, where $\omega_0 = 2\pi c / \lambda_0$ is the carrier frequency and λ_0 is the wavelength of the center of the laser spectrum. For TL pulses, the features in the MIIPS trace where the SHG signal is greatest form parallel lines separated by π . On the basis of this observation, we can restrict the search area of $\delta_m(\omega)$ for non-TL pulses. These black lines separating the MIIPS traces are shown in the left panels of Fig. 2.

For an analysis of a MIIPS trace, the $\delta_m^n(\omega)$ values in two neighboring areas are defined (as shown in the left

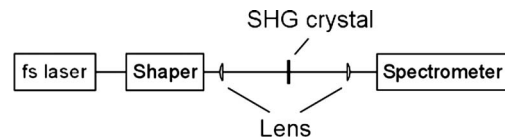


Fig. 1. Experimental MIIPS setup. fs, femtosecond.

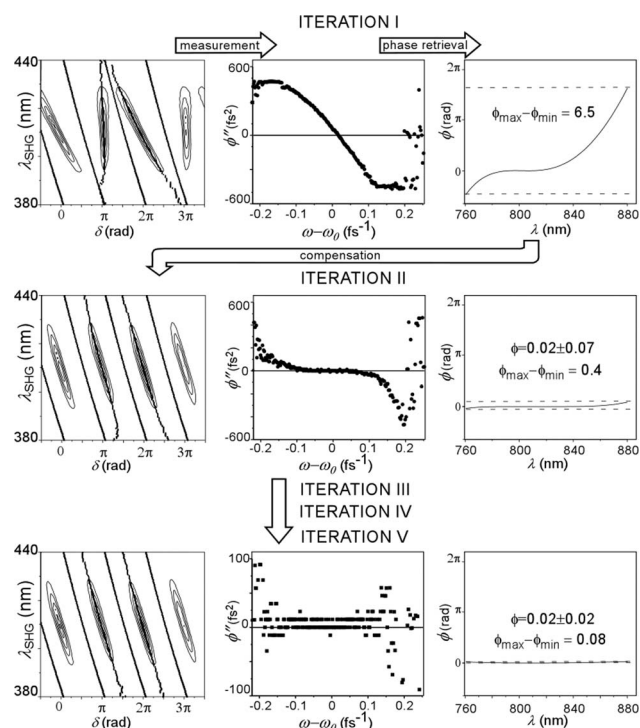


Fig. 2. Experimental demonstration of the MIIPS iteration process. The left panels are SHG spectra as the δ parameter of the reference function is scanned. Each vertical line corresponds to a separate SHG spectrum obtained at a given value for δ . The black lines that separate the MIIPS traces are used to define the region for searching $\delta_m(\omega)$. The dots within those boundaries show $\delta_m(\omega)$. The center panels show the retrieved second derivative of the spectral phase. The right panels show the phase calculated from the retrieved second derivative.

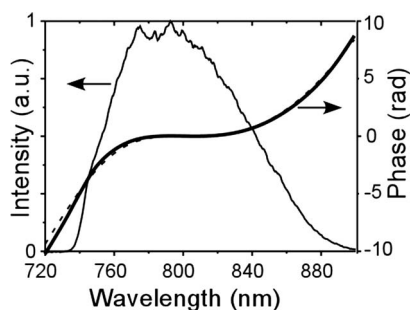


Fig. 3. Retrieved phase. The thick curve highlights the retrieved phase after five iterations, the dashed curve shows the retrieved phase from the first iteration, and the thin curve shows the spectrum of the laser pulse.

panels of Fig. 2) and used to calculate the second derivative of the unknown phase distortion:

$$\phi''(\omega) = \frac{1}{2} \alpha \gamma^2 \{ \sin[\gamma\omega - \delta_m^1(\omega)] + \sin[\gamma\omega - \delta_m^2(\omega)] \}. \quad (4)$$

The use of two lines (see Subsection 5.A) provides more accuracy in the measurements.

Given that the absolute accuracy of MIIPS improves as the magnitude of the phase distortions is reduced (see Subsection 5.B), an iterative procedure of measurement and compensation is used to obtain accurate results. The experiment begins as described above, and the phase is

retrieved. To compensate this distortion, $-\phi^I(\omega)$ is added to the phase using the pulse shaper, the process is repeated, and the next order of phase correction $\phi^{II}(\omega)$ is measured. The sum $-\phi^I(\omega) + \phi^{II}(\omega)$ is used as the correction function. The convergence toward an accurate result is exponentially fast and the phase distortion is close to zero after only three to five iterations. As shown in Fig. 2, the residue of the phase at the fifth iteration is very close to zero.

The unknown function $\phi(\omega)$ is accurately given by the sum of the iteratively determined compensation functions, $\phi_{\text{measured}} = \phi^I + \phi^{II} + \dots + \phi^N$. Figure 3 highlights the retrieved phase after five iterations for this measurement, as well as the phase retrieved from the first iteration. It shows that the first iteration already gives a good approximation of the phase distortion and the only significant deviation appears at the wings of the spectrum.

4. RESULTS

A. Reproducibility of Retrieved Phase

MIIPS was first tested for reproducibility. Several iterations of MIIPS were run to acquire a compensation mask (negative of the measured phase). This compensation mask was then applied, and a single iteration of MIIPS was run ten times successively (each time starting from the compensation mask). The retrieved phases were then analyzed for reproducibility. The solid curves in Fig. 4 are the average of all ten retrieved phases. The error bars in both panels show ± 1 standard deviation for every fifth point. The reproducibility of MIIPS is seen to be excellent over a range well exceeding that of the FWHM, as shown in the upper panel of Fig. 4.

To allow for a quantitative comparison of the reproducibility of MIIPS with other methods, the average of the standard deviations for each point was calculated using the power spectrum as a weighting function. Over the entire range of the spectrum, analyzing the full set of data, the statistical phase error was calculated to be 0.013 rad.

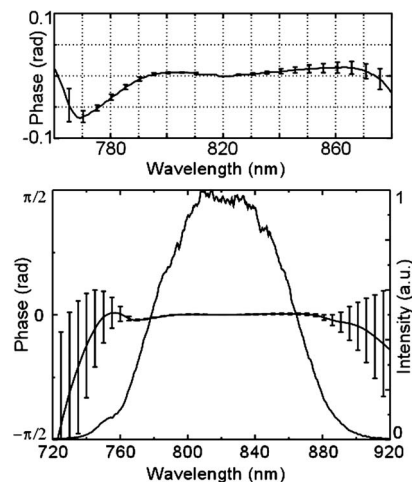


Fig. 4. Reproducibility of MIIPS. In both panels, the solid curve shows the average of ten independently retrieved phases, while the error bars show ± 1 standard deviation for every fifth point. The lower panel shows the full range of collected data. The upper panel shows a closer view of the region over which MIIPS can compensate (760–880 nm).

Table 1. Comparison of Reproducibility of MIIPS with FROG and SPIDER: Statistical Phase Error (in rad)

Method	Full Data Set	Reduced Data Set	Full Data Set (FWHM)
MIIPS	0.013	0.011	0.0028
FROG ^a	0.122	0.048	
SPIDER ^a	0.044	0.017	

^aRef. 40.

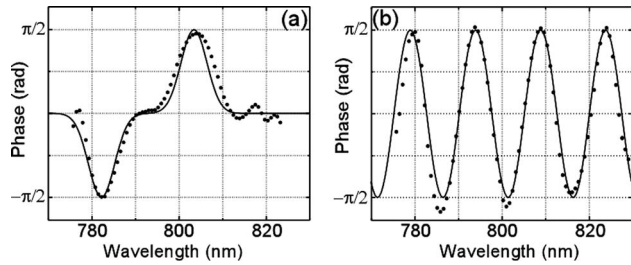


Fig. 5. Ability of MIIPS to retrieve arbitrary phase functions. (a) The result for an applied double Gaussian function. (b) The result for an applied sine function. The dotted curves show the retrieved phase, and the solid curves are the applied phase.

Using a reduced set of five scans, the statistical phase error was calculated as 0.011 rad. Table 1 compares these results with those reported by Gallmann *et al.* for FROG and SPIDER.⁴⁰ Also of interest is the great reduction of statistical phase error when the range of data analyzed was reduced to that in which the retrieved phase was flat (i.e., MIIPS had successfully compensated). For this range (shown in the upper panel of Fig. 4), the statistical phase error was reduced to just 0.004 rad. Additionally, some tasks, such as measuring group-velocity dispersion (GVD), do not require knowledge of the phase over a wide range. Within the FWHM of a pulse, MIIPS retrieves the phase with unprecedented precision: The statistical phase error is 0.0028 rad. These data lead us to conclude that MIIPS is a method with high reproducibility, exceeding that of FROG and SPIDER.

B. Accurate Retrieval of Applied Phase

The next step in testing the ability of MIIPS to retrieve arbitrary phase distortions was done by applying known phases to a TL pulse, running several iterations of MIIPS, and comparing the retrieved phase with the applied phase. We analyzed two different synthetic functions: a double Gaussian [results shown in Fig. 5(a)] and a sine function with amplitude $\pi/2$ and four periods across the SLM [results shown in Fig. 5(b)]. For these measurements, the pulses were first compensated to obtain TL pulses. The applied synthetic phase function was introduced, and the retrieved function was obtained. Note the good agreement between both the retrieved (dotted curve) and the applied phases (solid curve) in each case, indicating that MIIPS is capable of accurately retrieving an arbitrary phase from a pulse.

C. Effective Compensation of Retrieved Phase at the Target

To quantitatively test the accuracy of the MIIPS method to not only retrieve the arbitrary phase of a pulse, but to subsequently compensate for the measured phase distortions, MIIPS was used to acquire a TL pulse. A well-defined phase function was then introduced to the TL pulse, and the SHG spectrum was recorded. This spectrum was compared with the spectrum predicted by a theoretical application of the same phase function to a theoretically generated TL pulse. The results for two functions (a binary phase function and a sine function), chosen for their generation of multiple peaks, are shown in Fig. 6. Figures 6(a) and 6(c) illustrate excellent agreement between the experimentally obtained spectrum and the theoretical simulation with no adjustable parameters. In contrast, Figs. 6(b) and 6(d) show the resulting SHG spectrum when the same phase functions are applied to the uncompensated pulses. Clearly, phase distortions naturally present in the laser pulses cause significant changes in the nonlinear optical properties of the pulse and must be eliminated by accurate compensation. On the basis of the excellent match between the theoretically predicted and experimentally obtained SHG spectra, we conclude that MIIPS is capable of compensating phase distortions, and consequently eliminates the deleterious effects that the distortions have on nonlinear optical processes.

D. Accuracy in Measuring Group-Velocity Dispersion of a Material

To further quantitatively test the accuracy of the phases retrieved by MIIPS, we measured the GVD of quartz, a

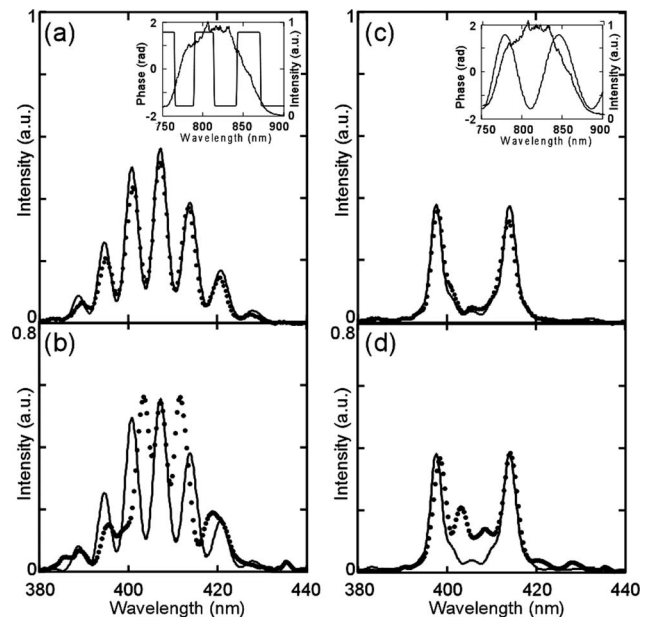


Fig. 6. Comparison between experimental data and theoretical simulation. The solid curve in each panel shows the theoretical spectrum predicted for the application of a particular binary phase (a) and (b) or a particular sine function (c) and (d). The dotted curves correspond to the experimentally measured SHG spectrum for each case. (a) The experimental result of the application of a binary phase mask (inset) to a pulse compensated by MIIPS. (b) The result of the application of the same phase mask to an uncompensated pulse. (c) and (d) The corresponding information using a sine function (inset).

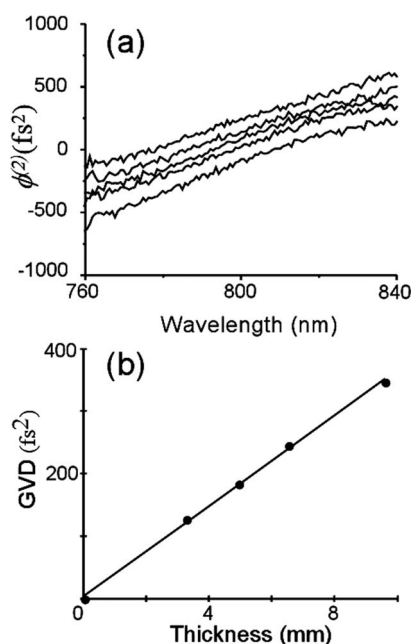


Fig. 7. GVD measurement of quartz using MIIPS. (a) The retrieved second derivative of the spectral phases (from bottom to top: 0, 3.25, 4.92, 6.53, and 9.58 mm quartz windows). (b) The GVD at 800 nm as a function of thickness.

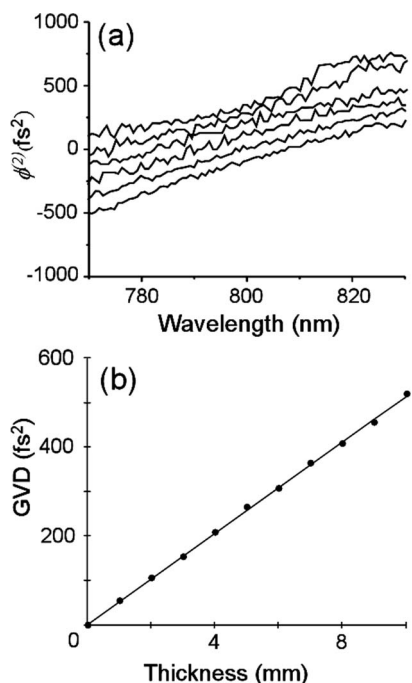


Fig. 8. GVD measurement of microscope slides using MIIPS. (a) The retrieved second derivative of the spectral phases (from bottom to top: 0, 2, 4, 6, 8, and 10 mm microscope slides). Note that for clarity the odd number of slides (odd thicknesses) were omitted from this graph, but not from the calculation. (b) The GVD at 800 nm as a function of thickness.

material for which the value has previously been measured by more conventional and accepted techniques. The beam was passed through quartz windows of thicknesses 3.25, 4.92, 6.53, and 9.58 mm before its incidence on the SHG crystal. MIIPS was used to compensate the pulses

and retrieve the second derivatives of the spectral phases of those pulses. The spectral phase was quantified, with the results from a MIIPS completed with no quartz present as a reference.

Figure 7(a) shows the retrieved second derivative of the spectral phase of the system for the different thicknesses of quartz. It is important to note that the curves are both parallel and spaced proportionally to the thickness of the quartz [as shown in Fig. 7(b)]. The GVD introduced by the quartz windows was measured to be 36.2 ± 0.5 fs²/mm at 800 nm, which is in good agreement with the 35.92 ± 0.05 fs²/mm measured by Diddams and Diels⁴¹ using white-light interferometry. For further comparison, the GVD of quartz at 800 nm was calculated using the Sellmeir formula and the constants found from Malitson⁴² and was found to be 36.162, which is in excellent agreement with our measured value.

We then repeated the measurement process, this time measuring the GVD of increasing numbers of glass microscope slides (crown glass, Fisher Scientific, each 1 mm thick). As the thickness of the slides is uniform, a reliable system for quantifying the GVD will show a linear plot of GVD versus the number of microscope slides.

The setup involved having the beam pass through the microscope slides, in place of the quartz windows. Nujol index-matching oil was used between them to avoid multiple reflections at the interfaces. Figure 8(a) shows the retrieved second derivatives of the spectral phase for every other slide addition. Figure 8(b) (all data shown) highlights the reliability of the MIIPS method. It can be seen that the experimentally measured GVD versus the number of microscope slides (thickness of glass) can be successfully fitted by a line. The GVD introduced by the microscope slides was measured at 50.7 ± 0.5 fs²/mm at 800 nm. Assuming the type of crown glass used for the microscope slides corresponds to Ohara glass S-NSL 5 (equivalent to Schott glass K5), we can compare our measured GVD with that calculated value using the Sellmeir formula with constants available from Ohara.⁴³ The GVD was calculated to be 50.13 fs²/mm at 800 nm, which is in good agreement with experiment.

E. Measurement, Compensation, and Reproducibility Through High-Numerical-Aperture Objectives

One of the greatest obstacles to fully developing the promising technique of multiphoton imaging is the significant amount of phase distortion introduced by high-numerical-aperture (NA) microscope objectives. To date, the characterization of such distortions has been accomplished for sub-10 fs pulses in objectives with a NA up to 0.85,⁴⁴ and for up to 1.30 NA objectives if longer pulses are used.^{45–48} Compensation of the quadratic term of the characterized distortions was accomplished in some cases through pre-compensation. However, higher-order phase distortions, introduced by the objectives and even by the prisms necessary to precompensate for the quadratic phase distortions, cannot be compensated by these methods, nor can the phase distortions be quantified. In this subsection, we demonstrate that MIIPS can successfully quantify and compensate for all orders of arbitrary phase distortions

introduced into a sub-10 fs pulse by high-NA microscope objectives.

For this procedure, a periscope was used to bring the laser beam into the rear port of a Nikon TE2000-U inverted microscope. The beam was reflected upward through the objective and focused onto the SHG crystal. The three objectives used were a Nikon Plan Fluor ELWD 20x/0.45 NA objective, a Nikon Plan Fluor ELWD 40x/0.60 NA objective, and a Nikon Plan Apo TIRF oil immersion 60x/1.45 NA objective (Nikon immersion oil, Type NF was used.).

MIIPS alone was sufficient to compensate for the phase distortions introduced by the 20x/0.45 NA and 40x/0.60 NA microscope objectives (results not shown). To allow for the best compensation of higher-order phase distortion introduced by the 60x/1.45 NA objective, a pair of SF10 prisms was used to reduce the quadratic phase contributions ($\sim 10^4$ fs²).

Figure 9 shows the compensation results for the 1.45 NA objective. In both panels, the solid curve shows the average phase residue from five independent measurements. The error bars show the ± 1 standard deviation for every fifth data point. The lower panel shows the full set of acquired data. The upper panel shows the same data over the FWHM with a reduced scale. Note that the phase is compensated to within 0.1 rad over the entire bandwidth of the pulse (770–860 nm), indicating that the distortions introduced by high-NA objectives are well compensated over that range. We highlight the extremely narrow standard deviation observed in the reduced range, providing evidence of a high degree of reproducibility of the MIIPS method, even when highly dispersive materials are utilized. The statistical phase error for the 60x/1.45 NA objective was calculated to be 0.026 rad over the full range of data, where the uncompensated phase distortion was ~ 100 rad. Considering the significant degree of distortion introduced by this high-NA objective, the precision by which phase is retrieved by MIIPS is excellent.

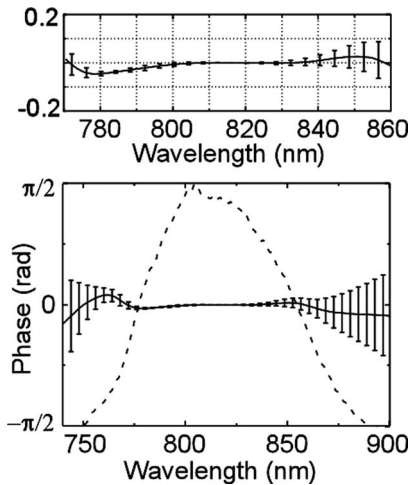


Fig. 9. Compensation of spectral phase distortions caused by a 60x/1.45 NA objective. The error bars indicate ± 1 standard deviation. The lower panel shows the full range of data, while the upper panel shows the same data over the FWHM of the pulse, on a reduced scale.

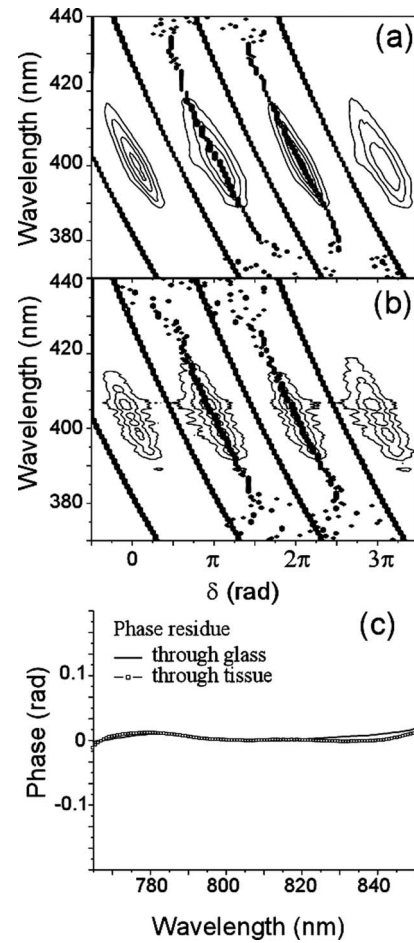


Fig. 10. MIIPS measurement through scattering biological tissue. (a) and (b) MIIPS traces without and with tissue, respectively. (c) While the overall signal-to-noise ratio is significantly decreased, similar phase information is obtained.

F. MIIPS Measurements after Transmission through Biological Tissue

When a laser beam transmits through a scattering medium like biological tissue, the coherent component of the electric field, although maintaining its directionality, degrades exponentially with tissue depth. This occurs as a result of the presence of macroscopic and microscopic cellular constituents, fat globules, and refractive-index mismatch between intracellular and extracellular fluids. Although femtosecond lasers have increasingly been used for medical diagnostics and therapeutics as well as for imaging applications, an underlying uncertainty exists as to the spectral phase distortions the laser pulse experiences as it propagates through several scattering lengths of tissue.

Here we tested the ability of the MIIPS method to measure spectral phase deformations caused by transmission through scattering biological tissue. The procedure involved measuring phase distortions inherent in a sub-10 fs laser pulse, correcting for these distortions to obtain TL pulses, and then comparing the spectral phase obtained when the laser transmits through a 500 μm slice of raw chicken breast tissue or through a similar thickness of glass. Preliminary experiments using a variable scattering medium (skim milk in water) (results not shown) in-

indicated that the retrieved spectral phases had little dependence, other than on the overall intensity, on the degree of scattering. This is indicative of the ability of the coherent component of the laser or the ballistic photons to maintain phase information as the laser penetrates a turbid scattering medium.³⁵ Our results with tissue (Fig. 10) confirm that, despite the presence of inhomogeneities that significantly affect the coherence of a femtosecond laser pulse, phase distortion is minimal. As expected, a reduction in signal-to-noise ratio resulting from the exponential decay of ballistic photons as the pulse transmits through several scattering lengths of tissue was observed. Notwithstanding this limitation, phase information is still comparable to that obtained when light goes through an optical medium like glass. Figures 10(a) and 10(b) show the MIIPS traces obtained for glass and tissue samples, respectively. The presence of tissue slightly decreases the range of wavelengths that can be compensated by MIIPS, but the fact remains that the method works. Figure 10(c) shows the phase residue, averaged over five trials, of the pulse as it went through glass and tissue. Note that the phase is compensated to within 0.02 rad over the entire FWHM of the pulse. With additional iterations, MIIPS can fully compensate for distortions introduced by a scattering medium. More significantly, the method corrects for distortions at the position of the sample.

Accurate phase compensation and accurate phase delivery is important. We have used this capability to perform selective functional imaging through biological tissue.³⁵ Simulations show⁴⁹ that even for signal-to-noise ratios as low as 1, it is possible to retrieve the spectral phase with high precision by smoothing the two-dimensional MIIPS data before analysis. The good resistance to noise and the fact that it is independent of mode quality are additional significant advantages of the MIIPS method, which is based on quasi-local phase compensation.

G. Dynamic Range

In this section, we determine the dynamic range of MIIPS for chirp compensation of the MIIPS method. At the low end, phase deviations over the entire bandwidth of the pulse (760–880 nm) are typically in the milliradian range: 0.02 rad (see Fig. 2). Higher sensitivity can be achieved through changes in the parameters α and γ and by introducing steps for the parameter δ that are smaller than the pixel size (see subsection 5.C). At 0.02 rad, MIIPS is already more sensitive than most of the established methods. At the high end of phase distortions, there is a point at which the MIIPS features in the trace coalesce and one can no longer measure a distance between them. This occurs when phase distortions are of the order of $\alpha\gamma^2$. Even in these cases, MIIPS is still capable of introducing a compensation phase that, after a number of iterations, corrects for very large phase distortions, as shown below.

When the phase modulation is greater than the total retardation allowed by the SLM, the phase is corrected by wrapping. Since the functional retardance of our SLM is limited to $\pm 2.6\pi$, we fold the spectral phase within a $\pm 1.1\pi$ range ($\pm 1.5\pi$ is reserved for the reference sine function). In Fig. 11 we show the compensation of a 40 fs pulse

from an amplified laser system that has been significantly chirped ($3 \times 10^4 \text{ fs}^2$) by the gratings in the internal compressor. Note that, despite significant wrapping of the phase [Fig. 11(b)], excellent compensation has been achieved, as can be judged by the residue phase [see upper panel of Fig. 11(a)].

The top end of the dynamic range is three times greater for the shaper used with the amplified system than for the sub-10 fs laser system on which most of the work was done (note that precompensation was necessary for the 1.45 NA objective). The range is limited by the optical design of the pulse shaper when we take into account the available number of pixels and the maximum retardation per pixel. Empirically, for the 128-pixel shapers, we find the upper dynamic range in ϕ''_{max} to be $\phi''_{\text{max}} = \phi_{\text{max}}\tau^2/4$, where ϕ_{max} is the maximum wrapping (in our case, 100 rad) and τ is the pulse duration. A similar estimation can be made for higher-order terms.

The spectral range of precise phase measurement and compensation is slightly less than the entire laser pulse spectrum. This is a limitation caused by the required generation of the second harmonic, and is common to all methods based on nonlinear optical processes. For extremely short pulses, when the bandwidth exceeds 100 nm FWHM, phase matching using a nonlinear optical crystal over the entire spectrum is a problem. This limit is independent of the phase characterization methods. However, compared with other methods, MIIPS is less restricted by this limit because of its low sensitivity to noise (discussed above). This allows the acquisition of good measurements where other methods might fail.

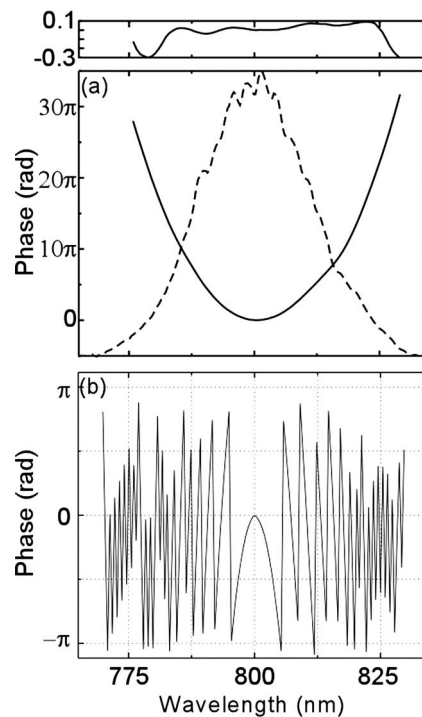


Fig. 11. Compensation of a heavily chirped pulse. (a) The retrieved phase of an uncompensated pulse. The upper panel shows the residue of the phase after successful compensation by MIIPS. (b) The applied compensation mask, with significant wrapping.

5. DISCUSSION

A. Using Two MIIPS Features Adds Stability and Accuracy

For small phase distortions, the second derivative near ω_0 is given by the average of two lines (see Fig. 2):

$$\begin{aligned} \phi''_{\text{measured}} &= \frac{1}{2} \alpha \gamma^2 [\sin(\xi + \epsilon_\phi) + \sin(-\xi + \epsilon_\phi + \pi)] \\ &\approx \left(1 - \frac{1}{2} \epsilon_\phi^2\right) \phi'' \end{aligned} \quad (5)$$

This sum has quadratic stability with respect to phase errors ϵ_ϕ . For a SLM with 128 pixels, and a phase function with one period across the spectrum, ϵ_ϕ is approximately 0.03 rad. The relative error of the two-line method is less than 0.001 rad, according to Eq. (5). In comparison, the relative error of a single-line analysis [when Eq. (3) is used instead of Eq. (4)] is approximately 0.03 rad. A similar analysis can be used to estimate the accuracy with respect to the measurements of frequency ϵ_ω . In this case,

$$\begin{aligned} \phi''_{\text{measured}} &= \frac{1}{2} \alpha \gamma^2 [\sin(\gamma \epsilon_\omega - \xi) + \sin(\gamma \epsilon_\omega - \xi + \pi)] \\ &\approx \left(1 - \frac{1}{2} \gamma^2 \epsilon_\omega^2\right) \phi'' \end{aligned} \quad (6)$$

An uncertainty of the spectral calibration of 1 nm gives ϵ_ω an approximate value of 0.003 fs⁻¹. According to Eq. (6), the relative error from this source is less than 0.001 rad for a 10 fs pulse.

B. Rationale for Iterative MIIPS

A single MIIPS scan is subject to some systematic deviations arising from the Taylor expansions of $\phi(\omega)$ and $f(\omega)$. The systematic error in the second derivative of $f(\omega)$ is approximately $1/12 \gamma^2 / \tau_0^2$, where τ_0 is the time duration of the pulse with the same spectrum. This single-scan error is $\sim 10\%$ when $\gamma^2 / \tau_0^2 \approx 1$. The sum of errors from all measured nonlinear terms of $\phi(\omega)$ define the error in the second derivative of the measured phase:

$$\phi''_{\text{measured}} \approx \phi'' \left(1 \pm \sum_n \frac{\phi^{n'}}{\tau_0^{2-n} n!}\right). \quad (7)$$

Errors in the measured phase come from high-order distortions, which enter Eq. (7) as $\phi^{n'}$, the n th derivative of the spectral phase. However, their contribution decreases with increasing order. Additionally, the greatest error is seen on the spectral wings of the pulse. The absolute error scales with the absolute value of phase distortion being measured. Therefore, as each iteration brings the pulse closer to TL, the absolute error associated with the retrieved phase decreases factorially.

C. Observation of Digital Noise

The digital noise of the retrieved ϕ'' (see center panel for iteration V in Fig. 2) is equal to $4\pi\alpha\gamma^2/N$, where N is the number of steps in the scan. The lower limit of the step size of the phase scan depends on the smallest possible phase delay introduced by the SLM and the number of

pixels in the SLM. In our case, these factors limit the digital noise in the second derivative measurements to 10 fs². Using a SLM with more pixels would provide even higher-accuracy spectral phase measurements, as a smaller step size could be used.

D. Spatial Considerations

Unlike all correlation-type techniques, the MIIPS method is not based on a space-to-time transformation. The main advantage is that it is insensitive to the spatial quality of the mode. Conversely, MIIPS does not account for pulse-front tilt that may be critical for certain time-resolved experiments. Spatial chirp has been found to affect the relative intensity, but not the position, of the features in MIIPS. When we observe this, we use an optical fiber coupled to a spectrometer to measure the spatial chirp and we correct it at the source.

6. CONCLUSION

We have carried out a series of quantitative tests on the reproducibility, reliability, accuracy, sensitivity, and dynamic range of the MIIPS method. MIIPS accomplished phase characterization, compensation of all orders of phase distortions, and accurate phase delivery. Because MIIPS can be carried out at the location of the sample, dispersions introduced by optics, high-NA microscope objectives, and even the sample itself can be corrected.

Our data show that the method is highly reproducible and accurate with a precision exceeding that of other phase measurement methods, and is capable of retrieving arbitrary phases. The accuracy was found to be 0.02 rad with a precision of 0.003 rad across the FWHM of the pulse. These values are superior to established methods, including SPIDER.⁴⁰ MIIPS was also found to accurately measure the GVD of quartz, glass, and highly scattering media.

The compensation and delivery of accurate spectral phase functions at the sample using MIIPS was confirmed by the excellent agreement between the experimentally recorded and the theoretically predicted SHG spectra for a continuous sine function and a discontinuous binary phase function. When the pulses were not compensated by MIIPS, significant deviations in the spectrum were observed.

The insensitivity of the MIIPS method to noise and beam quality was tested by transmitting the beam through biological tissue prior to the measurement. By comparing the result obtained when the beam was transmitted through 0.5 mm of glass or tissue, it was found that MIIPS reliably retrieved the spectral phase with an accuracy better than 0.02 rad across the FWHM of the pulse.

The dynamic range of MIIPS was tested by changing the spacing in the grating compressor of an amplified femtosecond laser. At the high end, the method successfully measured and compensated phase distortions up to 100 rad, this value being limited by the number of pixels in the shaper. With a 640-pixel shaper, this number can be multiplied by a factor of 5. For these large values of phase distortion, other phase characterization methods such as SHG FROG suffer from low signal-to-noise ratios. The

SPIDER method requires significant phase unwrapping to measure large phase distortions and an additional external method for compensation.

MIIPS can be used on diffuse beams and under poor signal-to-noise ratio conditions because it is a single-beam method that requires no overlap of beams in space and time. MIIPS does not use a retrieval algorithm; it is based on an analytical formula that directly provides the second derivative of the spectral phase. The integrated pulse shaper in MIIPS can simultaneously measure and compensate spectral phase distortions at the target. We are presently developing a method to obtain a MIIPS trace in a single laser shot that will provide valuable real-time characterization information. We conclude that MIIPS is an excellent choice for scientific and industrial applications involving femtosecond lasers.

ACKNOWLEDGMENTS

This work and Bingwei Xu were supported by the Major Instrument Development grant CHE-0421047 from the National Science Foundation. We are grateful for additional support from the Chemical Sciences, Geosciences and Biosciences Division, Office of Basic Energy Sciences, Office of Science, U.S. Department of Energy. We thank Igor Pastirk of Biophotonic Solutions Inc. for his help with the laser and pulse shaper systems.

REFERENCES

- V. V. Lozovoy, I. Pastirk, and M. Dantus, "Multiphoton intrapulse interference. IV. Ultrashort laser pulse spectral phase characterization and compensation," *Opt. Lett.* **29**, 775–777 (2004).
- J. M. Dela Cruz, I. Pastirk, V. V. Lozovoy, K. A. Walowicz, and M. Dantus, "Multiphoton intrapulse interference. 3: Probing microscopic chemical environments," *J. Phys. Chem. A* **108**, 53–58 (2004).
- R. Trebino and D. J. Kane, "Using phase retrieval to measure the intensity and phase of ultrashort pulses—frequency-resolved optical gating," *J. Opt. Soc. Am. A* **10**, 1101–1111 (1993).
- K. W. DeLong, R. Trebino, J. Hunter, and W. E. White, "Frequency-resolved optical gating with the use of second-harmonic generation," *J. Opt. Soc. Am. B* **11**, 2206–2215 (1994).
- R. Trebino, K. W. DeLong, D. N. Fittinghoff, J. N. Sweetser, M. A. Krumbugel, B. A. Richman, and D. J. Kane, "Measuring ultrashort laser pulses in the time-frequency domain using frequency-resolved optical gating," *Rev. Sci. Instrum.* **68**, 3277–3295 (1997).
- C. Iaconis and I. A. Walmsley, "Spectral phase interferometry for direct electric-field reconstruction of ultrashort optical pulses," *Opt. Lett.* **23**, 792–794 (1998).
- L. Gallmann, D. H. Sutter, N. Matuschek, G. Steinmeyer, U. Keller, C. Iaconis, and I. A. Walmsley, "Characterization of sub-6-fs optical pulses with spectral phase interferometry for direct electric-field reconstruction," *Opt. Lett.* **24**, 1314–1316 (1999).
- C. Dorrer, B. de Beauvoir, C. Le Blanc, S. Ranc, J. P. Rousseau, P. Rousseau, and J. P. Chambaret, "Single-shot real-time characterization of chirped-pulse amplification systems by spectral phase interferometry for direct electric-field reconstruction," *Opt. Lett.* **24**, 1644–1646 (1999).
- A. M. Weiner, "Femtosecond pulse shaping using spatial light modulators," *Rev. Sci. Instrum.* **71**, 1929–1960 (2000).
- A. M. Weiner, "Programmable shaping of femtosecond optical pulses by use of 128-element liquid-crystal phase modulator," *IEEE J. Quantum Electron.* **28**, 908–920 (1992).
- A. Assion, T. Baumert, M. Bergt, T. Brixner, B. Kiefer, V. Seyfried, M. Strehle, and G. Gerber, "Control of chemical reactions by feedback-optimized phase-shaped femtosecond laser pulses," *Science* **282**, 919–922 (1998).
- R. J. Levis, G. M. Menkir, and H. Rabitz, "Selective bond dissociation and rearrangement with optimally tailored, strong-field laser pulses," *Science* **292**, 709–713 (2001).
- C. J. Bardeen, V. V. Yakovlev, J. A. Squier, K. R. Wilson, S. D. Carpenter, and P. M. Weber, "Effect of pulse shape on the efficiency of multiphoton processes: implications for biological microscopy," *J. Biomed. Opt.* **4**, 362–367 (1999).
- D. Oron, N. Dudovich, D. Yelin, and Y. Silberberg, "Quantum control of coherent anti-Stokes Raman processes," *Phys. Rev. A* **65**, 043408 (2002).
- A. Neogi, H. Yoshida, T. Mozume, and O. Wada, "Enhancement of interband optical nonlinearity by manipulation of intersubband transitions in an undoped semiconductor quantum well," *Opt. Commun.* **159**, 225–229 (1999).
- J. Ahn, T. C. Weinacht, and P. H. Bucksbaum, "Information storage and retrieval through quantum phase," *Science* **287**, 463–465 (2000).
- V. V. Lozovoy and M. Dantus, "Photon echo pulse sequences with femtosecond shaped laser pulses as a vehicle for molecule-based quantum computation," *Chem. Phys. Lett.* **351**, 213–221 (2002).
- Y. Yasuno, M. Nakama, Y. Sutoh, M. Itoh, M. Mori, and T. Yatagai, "Optical coherence tomography by spectral interferometric joint transform correlator," *Opt. Commun.* **186**, 51–56 (2000).
- T. Baumert, T. Brixner, V. Seyfried, M. Strehle, and G. Gerber, "Femtosecond pulse shaping by an evolutionary algorithm with feedback," *Appl. Phys. B* **65**, 779–782 (1997).
- D. Meshulach, D. Yelin, and Y. Silberberg, "Adaptive real-time femtosecond pulse shaping," *J. Opt. Soc. Am. B* **15**, 1615–1619 (1998).
- A. Efimov, M. D. Moores, N. M. Beach, J. L. Krause, and D. H. Reitze, "Adaptive control of pulse phase in a chirped-pulse amplifier," *Opt. Lett.* **23**, 1915–1917 (1998).
- E. Zeek, K. Maginnis, S. Backus, U. Russek, M. Murnane, G. Mourou, H. Kapteyn, and G. Vdovin, "Pulse compression by use of deformable mirrors," *Opt. Lett.* **24**, 493–495 (1999).
- D. Zeidler, T. Hornung, D. Proch, and M. Motzkus, "Adaptive compression of tunable pulses from a non-collinear-type OPA to below 16 fs by feedback-controlled pulse shaping," *Appl. Phys. B* **70**, S125–S131 (2000).
- M. R. Armstrong, P. Plachta, E. A. Ponomarev, and R. J. D. Miller, "Versatile 7-fs optical parametric pulse generation and compression by use of adaptive optics," *Opt. Lett.* **26**, 1152–1154 (2001).
- A. Baltuska, T. Fuji, and T. Kobayashi, "Visible pulse compression to 4 fs by optical parametric amplification and programmable dispersion control," *Opt. Lett.* **27**, 306–308 (2002).
- F. L. Legare, J. M. Fraser, D. M. Villeneuve, and P. B. Corkum, "Adaptive compression of intense 250-nm-bandwidth laser pulses," *Appl. Phys. B* **74**, S279–S282 (2002).
- U. Siegner, M. Haiml, J. Kunde, and U. Keller, "Adaptive pulse compression by two-photon absorption in semiconductors," *Opt. Lett.* **27**, 315–317 (2002).
- A. Monmayrant, M. Joffre, T. Oksenhendler, R. Herzog, D. Kaplan, and P. Tournois, "Time-domain interferometry for direct electric-field reconstruction by use of an acousto-optic programmable filter and a two-photon detector," *Opt. Lett.* **28**, 278–280 (2003).
- B. Broers, H. B. V. Vandenheuvell, and L. D. Noordam, "Large interference effects of small chirp observed in 2-photon absorption," *Opt. Commun.* **91**, 57–61 (1992).
- K. A. Walowicz, I. Pastirk, V. V. Lozovoy, and M. Dantus, "Multiphoton intrapulse interference. 1. Control of multiphoton processes in condensed phases," *J. Phys. Chem. A* **106**, 9369–9373 (2002).

31. V. V. Lozovoy, I. Pastirk, K. A. Walowicz, and M. Dantus, "Multiphoton intrapulse interference. II. Control of two- and three-photon laser induced fluorescence with shaped pulses," *J. Chem. Phys.* **118**, 3187–3196 (2003).
32. M. Hacker, R. Netz, M. Roth, G. Stobrawa, T. Feurer, and R. Sauerbrey, "Frequency doubling of phase-modulated, ultrashort laser pulses," *Appl. Phys. B* **73**, 273–277 (2001).
33. I. Pastirk, J. M. Dela Cruz, K. A. Walowicz, V. V. Lozovoy, and M. Dantus, "Selective two-photon microscopy with shaped femtosecond pulses," *Opt. Express* **11**, 1695–1701 (2003).
34. J. M. Dela Cruz, I. Pastirk, M. Comstock, and M. Dantus, "Multiphoton intrapulse interference. 8. Coherent control through scattering tissue," *Opt. Express* **12**, 4144–4149 (2004).
35. J. M. Dela Cruz, I. Pastirk, M. Comstock, V. V. Lozovoy, and M. Dantus, "Use of coherent control methods through scattering biological tissue to achieve functional imaging," *Proc. Natl. Acad. Sci. U.S.A.* **101**, 16996–17001 (2005).
36. I. Pastirk, M. Kangas, and M. Dantus, "Multidimensional analytical method based on binary phase shaping of femtosecond pulses," *J. Phys. Chem. A* **109**, 2413–2416 (2005).
37. J. M. Dela Cruz, V. V. Lozovoy, and M. Dantus, "Quantitative mass spectrometric identification of isomers applying coherent laser control," *J. Phys. Chem. A* **109**, 8447–8450 (2005).
38. A. Baltuska, M. S. Pshenichnikov, and D. A. Wiersma, "Amplitude and phase characterization of 4.5-fs pulses by frequency-resolved optical gating," *Opt. Lett.* **23**, 1474–1476 (1998).
39. A. Baltuska, M. S. Pshenichnikov, and D. A. Wiersma, "Second-harmonic generation frequency-resolved optical gating in the single-cycle regime," *IEEE J. Quantum Electron.* **35**, 459–478 (1999).
40. L. Gallmann, D. H. Sutter, N. Matuschek, G. Steinmeyer, and U. Keller, "Techniques for the characterization of sub-10-fs optical pulses: a comparison," *Appl. Phys. B* **70**, (Suppl.) S67–S75 (2000).
41. S. Diddams and J. C. Diels, "Dispersion measurements with white-light interferometry," *J. Opt. Soc. Am. B* **13**, 1120–1129 (1996).
42. I. H. Malitson, "Interspecimen comparison of the refractive index of fused silica," *J. Opt. Soc. Am.* **55**, 1205–1209 (1965).
43. Ohara Corp., "Optical glass catalog data," retrieved May 2, 2005, <http://www.oharacorp.com/swf/catalog.html>.
44. J. Jasapara and W. Rudolph, "Characterization of sub-10-fs pulse focusing with high-numerical-aperture microscope objectives," *Opt. Lett.* **24**, 777–779 (1999).
45. I. Amat-Roldan, I. G. Cormack, P. Loza-Alvarez, and D. Artigas, "Starch-based second-harmonic-generated collinear frequency-resolved optical gating pulse characterization at the focal plane of a high-numerical-aperture lens," *Opt. Lett.* **29**, 2282–2284 (2004).
46. D. N. Fittinghoff, A. C. Millard, J. A. Squier, and M. Muller, "Frequency-resolved optical gating measurement of ultrashort pulses passing through a high numerical aperture objective," *IEEE J. Quantum Electron.* **35**, 479–486 (1999).
47. M. Muller, J. Squier, R. Wolleschensky, U. Simon, and G. J. Brakenhoff, "Dispersion pre-compensation of 15 femtosecond optical pulses for high-numerical-aperture objectives," *J. Microsc.* **191**, 141–150 (1998).
48. D. N. Fittinghoff, J. A. Squier, C. P. J. Barty, J. N. Sweetser, R. Trebino, and M. Muller, "Collinear type II second-harmonic-generation frequency-resolved optical gating for use with high-numerical-aperture objectives," *Opt. Lett.* **23**, 1046–1048 (1998).
49. V. V. Lozovoy and M. Dantus, "Systematic control of nonlinear optical processes using optimally shaped femtosecond pulses," *Chem. Phys. Chem.* **65**, 1952–1967 (2005).